Research Article Vol. 32, No. 9 / 22 Apr 2024 / Optics Express 16040
Optics EXPRESS

Chiral plasmonic metasurface assembled by DNA origami

NIELS GIESELER,[1,2] SVENJA MOENCH,[1] DOMINIK BEUTEL,[2] WOLFGANG G. PFEIFER,[3,4] CARMEN M. DOMÍNGUEZ,[1,*] CHRISTOF M. NIEMEYER,[1] AND CARSTEN ROCKSTUHL[2,5]

[1]*Institute of Biological Interfaces (IBG-1), Karlsruhe Institute of Technology, Hermann-von-Helmholtz Platz 1, 76344 Eggenstein-Leopoldshafen, Germany*
[2]*Institute of Theoretical Solid State Physics, Karlsruhe Institute of Technology, Kaiserstr. 12, 76131 Karlsruhe, Germany*
[3]*Department of Mechanical and Aerospace Engineering, The Ohio State University, 201 W. 19th Avenue, Columbus, 43210 Ohio, USA*
[4]*Department of Physics, The Ohio State University, 191 W. Woodruff Avenue, Columbus, 43210 Ohio, USA*
[5]*Institute of Nanotechnology, Karlsruhe Institute of Technology, Hermann-von-Helmholtz Platz 1, 76344 Eggenstein-Leopoldshafen, Germany*
[*]*carmen.dominguez@kit.edu*

Abstract: Chiral materials are essential to perceive photonic devices that control the helicity of light. However, the chirality of natural materials is rather weak, and relatively thick films are needed for noticeable effects. To overcome this limitation, artificial photonic materials were suggested to affect the chiral response in a much more substantial manner. Ideally, a single layer of such a material, a metasurface, should already be sufficient. While various structures fabricated with top-down nanofabrication technologies have already been reported, here we propose to utilize scaffolded DNA origami technology, a scalable bottom-up approach for metamolecule production, to fabricate a chiral metasurface. We introduce a chiral plasmonic metamolecule in the shape of a tripod and simulate its optical properties. By fixing the metamolecule to a rectangular planar origami, the tripods can be assembled into a 2D DNA origami crystal that forms a chiral metasurface. We simulate the optical properties but also fabricate selected devices to assess the experimental feasibility of the suggested approach critically.

1. Introduction

Optical metamaterials are artificial materials built from the periodic arrangement of structures that have a critical length scale smaller or ideally much smaller than the wavelength of light considered for operation. This results in physical properties of the metamaterial that are largely determined by the structure of the material units in combination with the intrinsic material properties of the units from which it is made. This combination makes it possible to create materials with on-demand properties that can be used to control the propagation of light in a precise manner as required for specific applications in a way that is not possible with naturally available materials [1]. While the notion of metamaterials emerged across all frequency spectra, ranging from static and low-frequency metamaterials up to the ultra-violet domain, we are particularly concerned here with optical metamaterials [2]. Moreover, the specific property of interest to us is that of chirality [3]. Chirality, per se, is a geometrical property. An object is chiral if it cannot be superimposed onto its mirror image. Geometrical chirality translates to a specific optical response where plane waves of different circular polarization propagating in a chiral medium obey different dispersion relations, i.e., different (complex) wavenumbers for a

#520522 https://doi.org/10.1364/OE.520522
Journal © 2024 Received 31 Jan 2024; revised 18 Mar 2024; accepted 18 Mar 2024; published 16 Apr 2024

Optics EXPRESS

given frequency [4]. Circular dichroism and optical rotation are two prominent effects that affect circularly polarized plane waves differently [5]. Both effects are at the heart of many applications revolving around controlling circular polarization states of light [6–8]. Circular polarizers and filters are crucial in photography, optical instrumentation, and display technologies, as they can selectively transmit or block circularly polarized light, improving image contrast and quality. The importance of materials that offer a large CD carries over to chiral sensing applications in biomedical sciences, where different enantiomers often have a highly different effect on the biological system. As current chiral sensing technologies are costly and require large amounts of samples, the field could benefit greatly from novel and more effective methods to control circularly polarized states of light [9,10]. However, the broken mirror symmetry in natural materials, usually molecules, happens on length scales much smaller than the optical wavelength. Consequently, the chiral optical response of natural materials is extremely weak. To effectively control circular polarization states of light, it is, therefore, crucial to design metamolecules with a strong chiral optical response [11]. These metamolecules will form a metamaterial or a metasurface upon a periodic arrangement in 3D or 2D, respectively [12].

We usually distinguish two different approaches to fabricate metamolecules. On the one hand, top-down approaches such as electron beam lithography, ion beam milling, or 3D laser printing can be used [13–15].

These approaches provide excellent deterministic control over the geometrical details of the structures resulting in a strong chiral optical response. However, top-down methods generally have slower production rates, are associated with higher production costs and usually only provide samples within a limited spatial area, thereby hampering large-scale applications [16]. Furthermore, true 3D structures are a notorious challenge, but one that is necessary to realize truly chiral objects and not just samples where mirror symmetry is broken by the presence of a substrate.

In contrast, bottom-up approaches overcome many of these limitations. Here, usually, self-assembly techniques are used to obtain photonic metamaterials of sufficient complexity that are feasible for large-scale fabrication at reasonably low costs [17,18]. As this research is motivated by its application in controling circular ploarized states of light, bottom-up approaches are, in this context, preferable to existing top-down methods. While many self-assembly strategies are known, few allow us to reach structures with a broken mirror symmetry, or at least not a racemic mixture. Moreover, by requiring a substantial optical response that prompts us to build resonant structures into the design that enhance the light-matter interactions, not many bottom-up fabrication avenues are left open. One of the most promising technologies is DNA-Nanotechnology [19,20].

The core idea of DNA-Nanotechnology [21–25] is to use the programmability of DNA strands, that is the predictable pairing of bases in DNA strands [26], to self assemble complex nanostructures. Since the creation of DNA-Nanotechnology by Seeman in 1982 [21], it was massively influenced by the development of Rothemund's DNA origami in 2006 [27] on which this work is based.

DNA origami [28,29] allows the creation of very complex structures [30–32]. By extending unpaired DNA linkers out of the DNA origami nanostructures, it is possible to position metallic nanoparticles functionalized with complementary DNA with nanometer precision [33]. This is essential for optical applications of DNA origami, as the intrinsic interaction of light and DNA is very weak due to the low contrast of the refractive index. Therefore, the plasmonic resonances of metallic nanoparticles are used to generate the necessary strong light-matter interaction. The combination of DNA and plasmonic nanoparticles has already been successfully used to create various plasmonic nanodevices, such as waveguides [34,35] or antennas [36]. Of special interest for our work on metamaterials are chiral plasmonic metamolecules assembled by DNA origami [37–40]. Also, the assembly of symmetric quasi-2D DNA origami into lattices is of interest,

Optics EXPRESS

which has been shown in solution [41–43] and at 2D liquid-lipid [44,45] and liquid-solid [46–48] interfaces.

While it has been proposed to combine these two results to create complex plasmonic metasurfaces [49], there exist only a few published results on DNA-based plasmonic [50,51] or silica-based [52] metasurfaces. To our knowledge, creating a chiral plasmonic metasurface has not been attempted. It is the purpose of this contribution to explore on computational grounds the possible optical response of a suitably optimized chiral plasmonic metasurface and to assess the feasibility of its fabrication on experimental grounds. Note that our approach differs from DNA origami placement methods that combine lithography with DNA origami [52,53], as this limits the periodicity of the metasurface. We stress upfront that we do not aim for a record-high optical response. Instead, we stay within the realm of experimentally accessible parameters and try to elucidate the potential of the technology.

The following work is structured into three sections. First, we introduce in Section 2 the considered chiral plasmonic metamolecule. This includes a study of its optical properties and an optimization of the plasmonic particle sizes. Second, we will consider in Section 3 a metasurface made from these plasmonic metamolecules and explore its optical properties. Finally, we will discuss in Section 4 the experimental feasibility of our suggested samples, where we show the realization of the necessary origami and the formation of a large ordered lattice.

2. Design metamolecule

In this section, we will discuss the chiral metamolecule at the core of our work. This metamolecule will then, in the next section, be used to create a chiral metasurface. The design of the metamolecule is shown in Fig. 1(a). It consists of the DNA origami, shown in blue, that forms a tripod, and the plasmonic particles, shown in gold, mainly responsible for the chiral response. The distance of the gold nanoparticles to the central axis shown in the orthographic projection is $d = 19.4\,\mathrm{nm}$, and the slant angle of the legs is $\beta = 35.3°$. The shape of a tripod was chosen as its legs allow for an ordered connection of the metamolecule to another DNA origami, which will be vital in forming a metasurface later on. We postpone the discussion of the origami to Section 4 and solely concentrate on the optical aspect for the time being. Note that while the DNA molecule is chiral, its chiroptical response is much lower than the response generated by the plasmonic nanoparticles. This is caused by the very similar refractive index of the DNA and its surrounding (water) solution, leading to a very low optical contrast. Therefore, the contribution of the DNA is neglected in the following simulations, where we only consider metamolecules made from a suitable spatial arrangement of metallic nanoparticles. The plasmonic particles considered in this work are three gold nanorods of different lengths. The length difference is necessary as, otherwise, the structure would be achiral. In the following, we optimize the lengths of these nanorods to achieve the highest chiroptical response possible with this setup. The considered lengths range between 20 nm and 50 nm with a step size of 2 nm. The diameter is 10 nm for all nanorods considered. Naturally, if the restriction on the shape of the nanoparticles and their discrete lengths is dropped, a better result can be reached. However, nanorods are the most basic shape for which three particles suffice to induce chirality, and a lower number of constituents is less prone to errors. Furthermore, the precision with which nanorods can be synthesized is limited, which explains the discrete lengths chosen in our optimization. The restrictions we place on ourselves here, therefore, correspond to an experimentally feasible metamolecule.

The figure of merit used for this work is the circular dichroism (CD), defined as the normalized difference between the absorption cross-section of the metamolecule for left- and righthand polarized light $\frac{\sigma_L - \sigma_R}{\sigma_L + \sigma_R}$. The CD is directly linked to the imaginary part of the parameter that characterizes the chiroptical response of the material. As the real and imaginary parts can be related to each other via a Kramers-Kronig relation, this gives the full information if a large enough spectrum is investigated. Additionally, we will examine the extinction cross-section

Optics EXPRESS

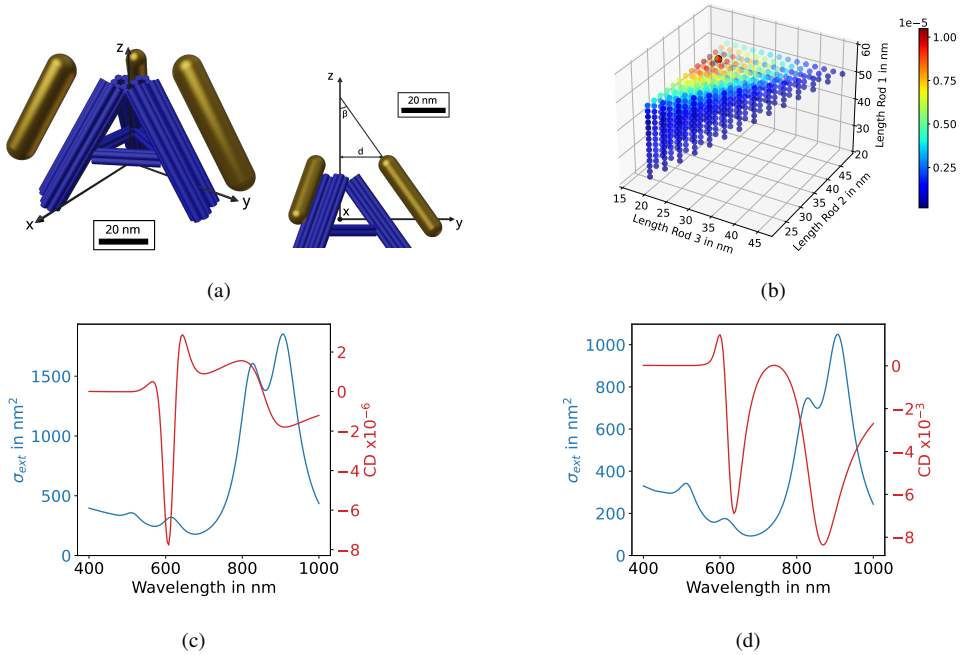

Fig. 1. (a) To scale representation of the metamolecule. The DNA origami is shown in blue and the three nanorods in gold. The orthographic projection on the right side shows the distance of the rods to the center d as well as the slant angle β. (b) The peak-to-valley difference in the orientational-averaged CD spectra for all examined structures. The length of the decorating particle for each leg is denoted on the x-, y-, and z-axis, respectively. The optimal structure with the highest peak-to-valley difference of the CD is marked in red and corresponds to the configuration shown in (a). (c) The simulated orientation-averaged optical response of the metamolecule that was shown in (a). The extinction cross-section is shown in blue, and the CD in red. (d) Extinction cross-section and CD of the metamolecule for a plane wave propagating in the $-z$-direction in blue and red, respectively.

averaged over both polarizations. For the optimization of the rod lengths, we are interested in the global quantities of the metamolecule and will consider cross-sections and CD that are rotationally averaged. This corresponds to an ensemble average to a specific illumination.

Details of the numerical simulations are documented in Supplement 1. In a nutshell, we initially use a finite-element method to retrieve the T-matrix of a given metamolecule from a larger number of full-wave simulations. We are specifically interested in the T-matrix in a helicity basis [54], which can be written as

$$\mathbf{T} = \begin{pmatrix} \mathbf{T}_{\mathrm{LL}} & \mathbf{T}_{\mathrm{LR}} \\ \mathbf{T}_{\mathrm{RL}} & \mathbf{T}_{\mathrm{RR}} \end{pmatrix}, \tag{1}$$

where the submatrices couple the different helicities to each other. Rotationally averaged quantities, such as the extinction cross-section, can easily be expressed as

$$\sigma_{\mathrm{ext}} = \frac{4\pi}{2k^2} \Re \left[\mathrm{Tr} \left(\mathbf{T}_{\mathrm{LL}} + \mathbf{T}_{\mathrm{RR}} \right) \right] . \tag{2}$$

Optics EXPRESS

Moreover, the rotationally averaged CD signal can be expressed as

$$\mathrm{CD} = \frac{\Re\left[\mathrm{Tr}\left(\mathbf{T}_{\mathrm{LL}}(\mathbf{1}-\mathbf{T}_{\mathrm{LL}}^{\dagger}) - \mathbf{T}_{\mathrm{RR}}(\mathbf{1}-\mathbf{T}_{\mathrm{RR}}^{\dagger})\right)\right]}{\Re\left[\mathrm{Tr}\left(\mathbf{T}_{\mathrm{LL}}(\mathbf{1}-\mathbf{T}_{\mathrm{LL}}^{\dagger}) + \mathbf{T}_{\mathrm{RR}}(\mathbf{1}-\mathbf{T}_{\mathrm{RR}}^{\dagger}) - \mathbf{T}_{\mathrm{LR}}^{\dagger}\mathbf{T}_{\mathrm{LR}} - \mathbf{T}_{\mathrm{RL}}^{\dagger}\mathbf{T}_{\mathrm{RL}}\right)\right]}, \tag{3}$$

where k is the wave number of the incident wave, and † denotes the Hermitian conjugate [55]. Note that due to the average, the orientation of the incident wave has no influence on the result.

We will now look at the peak-to-valley difference of the rotationally averaged CD in the spectral region of interest (400-1000 nm). Instead of the absolute maximum, we chose the difference from peak to valley, as this should lead to spectra with a more dispersive line shape. These spectra are easier to detect experimentally at low yields. The optimization results are shown in Fig. 1(b) as a scatter plot, where the position along the three dimensions corresponds to the length of the three nanorods. The color of each data point shows the peak-to-valley difference of the CD. The configuration with the highest peak-to-valley difference of the CD is highlighted by the slightly larger, bright red point and is the configuration shown in Fig. 1(a).

As a general trend, the CD decreases when the constituents get smaller, that is, when one moves toward the bottom left-hand corner of the figure. This is not due to the overall scattering decreasing, as the CD is normalized to the scattering response. An intuitive reason for this might be that the more different the lengths of the three nanorods are, the higher is the chirality of the tripod. One should, however, be careful with such interpretations as there is no definite quantization scheme for chirality [56], and the geometrical chirality does not necessarily coincide with that of the plasmonic mode [57]. Indeed, what eventually matters is the chiral interaction of light with the structure [58].

Having found the optimal structure of our metamolecule that will be used in the following, we now study this configuration in more detail. The lengths of the nanorods for the optimal configuration are 22 nm, 42 nm, and 50 nm. The resulting rotationally averaged CD and extinction cross-section spectra for this tripod are shown Fig. 1(c) in red and blue, respectively. The extinction cross-section shown here and in all further plots is the average of both polarizations. The spectrum shows four distinct peaks that can be connected to the plasmonic resonances of the constituents. The first resonance at roughly 500 nm corresponds to the transversal resonance of the nanorods. As the transversal resonance only varies slightly with the length of the nanorods, this results in one single, albeit broadened, resonance. The three following resonances are the longitudinal resonances of the three nanorods in increasing order of their length.

This direct correspondence shows that the spectrum can be explained as the superposition of its constituents, along with some mild hybridization between the plasmonic modes sustained in each nanorod. The hybridization is important, as each nanorod would be mirror-symmetric, and only the collective response enables a chiral response. Clearly, the design is necessarily a compromise that balances multiple and mutually exclusive demands. On the one hand, theory suggests that a strong hybridization can only be reached for particles with comparable resonance frequencies [59]. On the other hand, if the nanorods have similar lengths to hybridize their plasmonic modes properly, the metamolecule is not sufficiently chiral to cause a strong response, as discussed earlier. In each case, the systematic analysis on numerical grounds permits an optimization within the parameter range feasible for an experimental realization.

Theoretically speaking, there are several possibilities to improve the plasmonic hybridization and, thus, to increase the CD. For example, the resonances of the nanorods could be tailored by coating the nanorods with another metal, achieving similar resonances while retaining different shapes of the particles. However, precise control over this is experimentally not feasible. An alternative would be the usage of nanospheres where the resonance does vary more slowly with the size. However, this would require at least four particles that have to be placed at distinctive

Optics EXPRESS

positions, which would complicate the physical assembly of the metamolecule. For the following study, this configuration with three nanorods is therefore used.

While the ensemble average is a more complete measure of the properties of the metamolecule, the goal is the formation of a metasurface where the metamolecules are arranged in a fully ordered fashion. Therefore, we will now study the extinction cross-section and the CD for a single specific direction of incidence. We choose propagation in the $-z$-direction in correspondence to the illumination used later for the metasurface. Note, that while we fix the direction of incidence to a single value, the outgoing waves are still averaged over the entire space when considering the response of an individual metamolecule. This configuration, which is more reminiscent of the setup of the metasurface instead of the orientation averaged CD, could have been further optimized. However, differences in the predicted optimal geometry are minimal (see Fig. S1), and the orientation average leads to a more fundamental property of the metamolecule.

The resulting spectra of the extinction cross-section and CD are shown in Fig. 1(d) in blue and red, respectively. The extinction cross-section does only change quantitatively. The height of the longitudinal peaks is reduced compared to the ensemble average because the average included states in which the resonances of the rods were maximally excited. The change in the CD spectrum appears more drastic. However, the qualitative behavior of the modes is retained. The minima at 640 nm and 870 nm appear in both spectra but are much more pronounced in the unaveraged spectrum and, therefore, overlay the double-peak structure between them. Note also that the CD is three orders of magnitude greater when illuminated from this specific orientation. This might be due to the orientation providing a high geometrical chirality.

3. Metasurface

Having discussed the response of a single metamolecule, we will now turn to the periodic arrangement of the metamolecules in a metasurface. To this end, the tripod is attached to a second planar rectangular origami nanostructure, that we will refer to as the baseplate in the following. The periodicity of the metasurface is determined by the width and length of the baseplate. The quasi-two-dimensional DNA origami baseplate used in this study was chosen as a standardized component because it corresponds to typical dimensions of DNA origami objects [60,61] resulting in a periodicity of $\sim$ 100 nm. We note that, in principle, other dimensions can also be achieved using DNA origami, which should then lead to different periodicities and altered scattering behavior. In general, the chiral response strength of the periodically arranged scatterers should increase linearly with the scatterer density. At higher densities, however, the lattice interaction increases, which makes a general estimation of the response difficult. Note that this approach justifies the more complicated design of our plasmonic metamolecule compared to other designs reported, as our design features three legs that can be bound stably to such a baseplate. Furthermore, the usage of fully chiral plasmonic metamolecules as the basis of the metasurface results in a metasurface which is inherently chiral. This is preferable to a more simple arrangement of nanoparticles placed planar on the baseplates where the symmetry would only be broken in the presence of a substrate. A representation of the resulting metasurface is shown in Fig. 2(a).

The optical response of this metasurface at normal incidence was calculated using a finite element solver using periodic boundary conditions. For this calculation, the substrate was neglected as it would only mask the desired information. For a metasurface, the definition of the CD given earlier makes little sense, as the transmission coefficient T replaces the cross-section σ. Furthermore, we will only examine normal incidence in the following. Therefore, we turn to the transmission CD, defined as $\frac{T_\mathrm{L}-T_\mathrm{R}}{T_\mathrm{L}+T_\mathrm{R}}$, to quantify the chiral optical response of the structure [62]. Note that we will refer to the transmission CD as CD in the following for brevity.

The resulting spectra for a downwards propagating wave at normal incidence are shown in Fig. 2(b). The transmission spectrum shows the average over both polarizations. Note that $1-T$ is

Optics EXPRESS

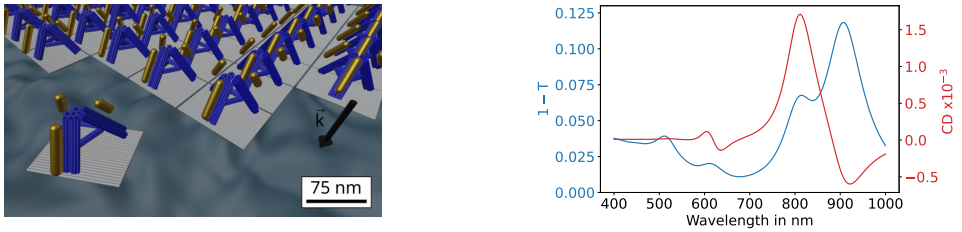

(a) (b)

Fig. 2. (a) Representation of the metasurface. The tripod is shown in blue, the baseplate in white, and the gold nanoparticles in gold. The direction of the illumination is indicated in black. (b) Optical response of the metasurface. The transmittance is shown in blue and the transmission CD in red.

shown instead of T to improve readability. The transmission spectrum shown in blue is generally close to unity. That can be easily explained by the rather low density of plasmonic scatterers. This is a general restriction of our method. While a very high periodicity of structures can be reached, the amount of plasmonic material is limited due to the DNA scaffolds being the main part of the metamolecule. The transmission through such a metasurface will, therefore, always be comparatively high. The four resonances in the spectrum can again, as for the metamolecule, be connected to the resonances of the single nanorods, which is expected as the surface is composed of the metamolecules.

The spectrum of the CD in red differs from the CD spectrum of the single metamolecule for a specific illumination, shown in Fig. 1(d). As the incident wave is propagating in the $-z$-direction in both cases, this difference can be explained by two reasons. On the one hand, the emerging lattice interaction renormalizes the polarizabilities of the tripod ensemble. This causes a change in the polarizability of the particle and, as such, causes a different optical response. On the other hand, whereas previously we studied scattering for a fixed illumination into all possible directions, the examination of a metasurfaces forces us to consider only the optical response into a single direction. Since the current metasurface has a subwavelength period, only a zeroth-order exists in the transmission that propagates in the same direction as the illumination. Both effects cause a change in the response. Nevertheless, the position of the peaks in the CD spectrum is still the same as before. The only change is that the peak at 800 nm, which is also visible in the ensemble average in Fig. 1(c), is not overruled here by the minima that governed the spectrum for a fixed illumination in Fig. 1(d). Of special interest is the bisignate line shape of the CD spectrum at 600 nm which matches to the resonance of the 22 nm rod. This is characteristic for a Born-Kuhn type systems [63]. Note that this line shape is already present in the response of a single metamolecule in Figs. 1(c) and 1(d). The other bisignate line shape from 750 nm to 1000 nm is most likely the result of the interference of two Born-Kuhn type modes, one for each rod.

While the CD achieved by our design is smaller than those achieved by top-down approaches in similar spectral regions [64–66], our method can create much higher densities of metamolecules. Therefore, with further improvements, the results of top-down approaches could be matched. In addition, the scalability of self-assembly methods offers a clear advantage over top-down methods. Furthermore, one needs to emphasize the modularity of our approach as an additional advantage. With the design proposed here, both the baseplate and the metamolecule can be modified or exchanged separately from each other, leading to a more simple adjustment of key parameters.

Optics EXPRESS

4. Experimental feasibility

Having explored the possible optimized structures that would be in reach with the considered DNA-Nanotechnology, we would now like to present our assessment of experimental feasibility. To this end, we will show the assembly of the tripod, the connection between the tripod and the baseplate, and the assembly of a large ordered lattice out of the baseplates.

The design of the tripod is based on published results [67]. Each of the three legs comprises a 14-helix bundle in a honeycomb lattice. The connecting struts are 4-helix bundles in a square lattice to adjust the tripod to the desired angle. The tripod has between 8 and 14 extensions out of each leg, depending on the nanorod length designed to bind. Additionally, each leg has two extensions to bind to the baseplate. The extensions are shown and discussed in more detail in Fig. S2.

The tripod was assembled by folding a single-stranded DNA molecule, the commercially available p8064 scaffold strand, with 234 staple strands. Successful folding was validated by agarose gel electrophoresis (See Fig. S3a) and atomic force microscopy (AFM). An AFM image of successfully fabricated tripods is shown in Fig. 3(a). The origami was assembled as designed, with the three legs clearly visible. The distortions that appear for some tripods are most likely artifacts from the tripod collapsing on the 2D mica surface during deposition for imaging.

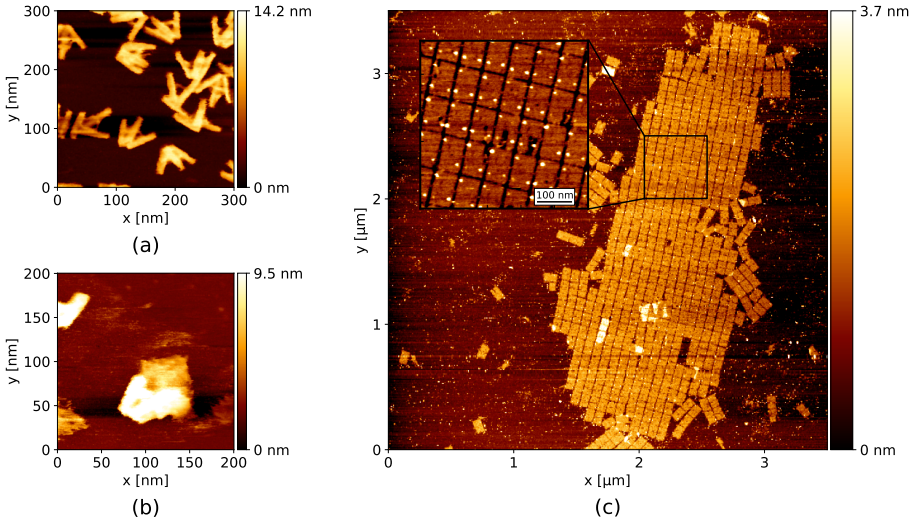

Fig. 3. AFM images of tripods (a), a tripod hybridized to a baseplate via Watson-Crick base-pairing (b), and a lattice formed out of baseplates (c). The inlay shows a magnified part of the lattice where the protein streptavidin was bound to the baseplates as a topographical marker to visualize the rotation of the singular plates. The scalebar in the inlay indicates 100 nm.

With the tripod assembly demonstrated, we will now turn to the baseplate. The origami is a modified version of a structure reported earlier [60,61]. It consists of a single 24-helix monolayer and is, therefore, fully planar once adsorbed to mica. The modification consists of six extensions to anchor the tripod, six biotinylated staples to bind streptavidin [60] to be used as a topographic marker, and 14 extensions at the edge of the origami to bind the baseplates in a lattice. The linking system is represented in Fig. S2. The baseplate is formed out of a p7560 scaffold and 238 staple strands. The origami was again characterized using agarose gel electrophoresis and AFM (see Fig. S3) and formed as designed.

The connection of the tripod to the baseplate is vital to pass the order of the lattice of baseplates onto the tripods and, therefore, to the plasmonic particles. This Watson-Crick hybridization is

Optics EXPRESS

performed by mixing the two origami structures at 37 °C to dissolve unspecific connections that might arise from the other extensions in the design. The connection of the origami was analyzed using AFM. One such successful hybrid structure is shown in Fig. 3(b). The tripod with its thicker legs appears more brightly in the image than the flat baseplate. Because the tripod is placed on top of the baseplate, only the top half of the baseplate is clearly visible. The relative position of the two origami to each other is as designed.

With this, the final step in creating a metasurface is the creation of the baseplate lattice. As the response of the metasurface depends on a uniform orientation of each baseplate, edge-specific linking strands have to be used as primary binding force instead of close packing or blunt-end stacking. To additionally discourage line defects, fully unique sequences with 10 binding base pairs are used. The sequence length was carefully tailored to avoid aggregation during origami formation while remaining long enough to bind the lattice together stably. Because of the specificity of the strands, surface-assisted methods, where the lattice is formed after adsorption to a 2D substrate, cannot be employed. This is because the baseplates can adsorb to the substrate in two ways, directly leading to two competing lattices and reducing the overall quality of the lattice. We, therefore, follow the route of forming the lattice in solution via slow thermal annealing, similar to [42].

The baseplates are thermally annealed from 46 °C to 4 °C over 126 hours. A representative lattice is shown in Fig. 3(c). The lattice shown is about 3.5 µm long and 1 µm wide with length and width correlating with the shape of the baseplate. Lattices with up to 5 µm length were observed (see Fig. S4a). However, the width was generally lower. This is expected, both because of the aspect ratio of the baseplate and because there are fewer linkers along the long side of the origami than on the short side.

The quality of the lattice is further examined by adding streptavidin to the formed lattice. The streptavidin binds to the biotinylated staples placed at three of the four corners of the baseplate. The asymmetric location allows us to discern the rotation of each baseplate. The binding is facilitated using two staples per streptavidin to obtain a stronger binding, as shown in Fig. S2.

The additional height of the streptavidin molecules can be used as a topographic marker, seen as three bright points on each baseplate in the zoomed-in inlay of Fig. 3(c). The inlay shows that the lattice quality is very high, with no line faults or missing plates. The small defects observed in the inset on some base plates are most likely an artifact due to the mechanical stress caused by the repeated imaging with the AFM tip, and can, therefore, be ignored as they are not inherent to the production process.

All plates with full streptavidin occupancy are oriented the same way. As the binding rate is not 100%, the orientation is unclear for some baseplates. However, there is no baseplate with streptavidin in the top right-hand corner, which would indicate the other rotation. The orientation and quality of the lattice are retained over much larger distances than shown here, compare Fig. S4b.

5. Conclusion

Chiral metasurfaces are an active area of research. However, most approaches would face serious problems with eventual applications due to their low scalability.

In this paper, we have proposed a chiral plasmonic metasurface assembled by DNA origami, which, as a self-assembly method, shows high scalability. This was done by combining the abilities of DNA origami to form complex metamolecules and well-ordered lattices.

We proposed a DNA origami tripod decorated with gold nanorods as a chiral metamolecule, and we optimized the size of the nanoparticles regarding the simulated CD of the metamolecule in solution. We then simulated the optical response of the tripod arranged in a regular metasurface with a periodicity of ~100 nm. Our results indicate a low hybridization between the plasmonic

Optics EXPRESS

particles. This results in a smaller CD than realized with other methods. However, due to the high density of metamolecules, our approach can potentially match these results.

Additionally, we investigated the feasibility of our proposed method by performing key steps of the fabrication process. We showed the successful formation of the two DNA origami, that form the scaffold for the plasmonic particles. The first origami is a tripod, which is needed to form the chiral plasmonic metamolecule. The second origami is a rectangular baseplate that can be assembled into a large regular lattice using linking strands. We achieved high-quality lattices on a micrometer scale, with up to 5 µm along one dimension. Lastly, we showed the possibility of hybridizing the tripod to the baseplate, thus enabling us to transfer the order of the lattice to the chiral metamolecule.

The final step in the formation of a chiral plasmonic metasurface involves the decoration of the tripod with gold nanoparticles. Based on literature work [67–69], this should be experimentally feasible, as the sequence design of the DNA linker strands should ensure a sufficiently high specificity for the selective linkage of the components. Although initial investigations into the assembly of the components showed that the decoration of the origami tripod with gold nanoparticles works in principle (Fig. S5), there were major problems with the aggregation of the particulate components in particular, which could not be solved either by extensive variation of annealing time and temperature or by adding detergents or carrying out intermediate purification steps. We suspect that the physico-chemical stability of the DNA-modified gold particles, in particular, is the cause of the problems. Therefore, this study suggests that there is still a great need for research and development of robust metallic nanoparticles before such bottom-up approaches can be used for routine processes. While this would be the main challenge for future investigations, it might also be worthwhile to first reinvestigate the tripod as the scaffold of the chiral plasmonic metamolecule. By placing the gold nanoparticles closer together, stronger interactions and, thus, stronger CD values could be reached. However, this would require either redesigning the tripod or switching to a different origami altogether.

While there remain open questions, we have shown the feasibility of assembling chiral plasmonic metasurface by DNA origami, a method that, due to its scalability and modularity, is particularly geared towards eventual applications.

Funding. Deutsche Forschungsgemeinschaft (EXC – 2082/1 – 390761711, SFB 1173 – Project number 258734477); Carl-Zeiss-Stiftung (CZF-Focus@HEiKA); Helmholtz Association (Materials Systems Engineering); Karlsruhe Institute of Technology (Virtual Materials Design); Fonds der Chemischen Industrie (Kekulé fellowship).

Acknowledgments. We thank Prof. Barbara Saccà for helpful support in the early phase of the project. The authors are grateful to the company JCMwave for their free provision of the FEM Maxwell solver JCMsuite.

Disclosures. The authors declare that they have no known competing financial interests or personal relationships that could have appeared to influence the work reported in this paper.

Data availability. Data underlying the results presented in this paper are not publicly available at this time but may be obtained from the authors upon reasonable request.

Supplemental document. See Supplement 1 for supporting content.

References

1. M. Kadic, G. W. Milton, M. van Hecke, *et al.*, "3d metamaterials," Nat. Rev. Phys. **1**(3), 198–210 (2019).
2. N. I. Zheludev and Y. S. Kivshar, "From metamaterials to metadevices," Nat. Mater. **11**(11), 917–924 (2012).
3. I. Fernandez-Corbaton, C. Rockstuhl, and P. Ziemke, "New twists of 3d chiral metamaterials," Adv. Mater. **31**(26), 1807742 (2019).
4. V. K. Valev, J. J. Baumberg, C. Sibilia, *et al.*, "Chirality and chiroptical effects in plasmonic nanostructures: Fundamentals, recent progress, and outlook," Adv. Mater. **25**(18), 2517–2534 (2013).
5. M. L. Solomon, A. A. E. Saleh, and L. V. Poulikakos, "Nanophotonic platforms for chiral sensing and separation," Acc. Chem. Res. **53**(3), 588–598 (2020).
6. P. Scott, X. Garcia-Santiago, and D. Beutel, "On enhanced sensing of chiral molecules in optical cavities," Appl. Phys. Rev. **7**(4), 041413 (2020).
7. M. Hanifeh, M. Albooyeh, and F. Capolino, "Optimally chiral light: Upper bound of helicity density of structured light for chirality detection of matter at nanoscale," ACS Photonics **7**(10), 2682–2691 (2020).

Optics EXPRESS

8. J. García-Guirado, M. Svedendahl, J. Puigdollers, *et al.*, "Enhanced chiral sensing with dielectric nanoresonators," Nano Lett. **20**(1), 585–591 (2020).
9. A. Guglielmelli, G. Palermo, and G. Strangi, "Unveiling chirality: Exploring nature's blueprint for engineering plasmonic materials," MRS Commun. **13**(5), 704–713 (2023).
10. A. Guglielmelli, G. Nicoletta, and L. Valente, "Numerical modeling of 3d chiral metasurfaces for sensing applications," Crystals **12**(12), 1804 (2022).
11. L. Lin, S. Lepeshov, and A. Krasnok, "All-optical reconfigurable chiral meta-molecules," Mater. Today **25**, 10–20 (2019).
12. L. Kühner, F. J. Wendisch, and A. A. Antonov, "Unlocking the out-of-plane dimension for photonic bound states in the continuum to achieve maximum optical chirality," Light: Sci. Appl. **12**(1), 250 (2023).
13. X. Lu, X. Wang, S. Wang, *et al.*, "Polarization-directed growth of spiral nanostructures by laser direct writing with vector beams," Nat. Commun. **14**(1), 1422 (2023).
14. R. R. Jones, C. Miksch, and H. Kwon, "Dense arrays of nanohelices: Raman scattering from achiral molecules reveals the near-field enhancements at chiral metasurfaces," Adv. Mater. **35**(34), 2209282 (2023).
15. K. Höflich, R. B. Yang, and A. Berger, "The direct writing of plasmonic gold nanostructures by electron-beam-induced deposition," Adv. Mater. **23**(22-23), 2657–2661 (2011).
16. J. Karst, M. Hentschel, N. H. Cho, *et al.*, "Chiral plasmonics," in *Plasmonic Materials and Metastructures*, S. Gwo, A. Alù, X. Li, and C.-K. Shih, eds. (Elsevier, 2024), Chapter 10, pp. 285–317.
17. X. Lan and Q. Wang, "Self-assembly of chiral plasmonic nanostructures," Adv. Mater. **28**(47), 10499–10507 (2016).
18. J. Lv, X. Gao, and B. Han, "Self-assembled inorganic chiral superstructures," Nat. Rev. Chem. **6**(2), 125–145 (2022).
19. C. Zhou, X. Duan, and N. Liu, "DNA-nanotechnology-enabled chiral plasmonics: From static to dynamic," Acc. Chem. Res. **50**(12), 2906–2914 (2017).
20. A. Kuzyk, M. J. Urban, and A. Idili, "Selective control of reconfigurable chiral plasmonic metamolecules," Sci. Adv. **3**(4), e1602803 (2017).
21. N. C. Seeman, "Nucleic acid junctions and lattices," J. Theor. Biol. **99**(2), 237–247 (1982).
22. N. C. Seeman, "DNA engineering and its application to nanotechnology," Trends Biotechnol. **17**(11), 437–443 (1999).
23. N. C. Seeman, "DNA in a material world," Nature **421**(6921), 427–431 (2003).
24. N. C. Seeman, "DNA enables nanoscale control of the structure of matter," Q. Rev. Biophys. **38**(4), 363–371 (2005).
25. M. R. Jones, N. C. Seeman, and C. A. Mirkin, "Programmable materials and the nature of the DNA bond," Science **347**(6224), 1260901 (2015).
26. J. D. Watson and F. H. C. Crick, "Molecular structure of nucleic acids: A structure for deoxyribose nucleic acid," Nature **171**(4356), 737–738 (1953).
27. P. W. K. Rothemund, "Folding DNA to create nanoscale shapes and patterns," Nature **440**(7082), 297–302 (2006).
28. S. Dey, C. Fan, and K. V. Gothelf, "DNA origami," Nat. Rev. Methods Primers **1**(1), 13 (2021).
29. B. Saccà and C. M. Niemeyer, "DNA origami: The art of folding DNA," Angew Chem. Int. Ed. **51**(1), 58–66 (2012).
30. M. DeLuca, W. G. Pfeifer, and B. Randoing, "Thermally reversible pattern formation in arrays of molecular rotors," Nanoscale **15**(18), 8356–8365 (2023).
31. A. Mills, N. Aissaoui, and D. Maurel, "A modular spring-loaded actuator for mechanical activation of membrane proteins," Nat. Commun. **13**(1), 3182 (2022).
32. E. Benson, R. C. Marzo, J. Bath, *et al.*, "A DNA molecular printer capable of programmable positioning and patterning in two dimensions," Sci. Robot. **7**(65), eabn5459 (2022).
33. A. Kuzyk, R. Jungmann, G. P. Acuna, *et al.*, "DNA origami route for nanophotonics," ACS Photonics **5**(4), 1151–1163 (2018).
34. K. Vogele, J. List, and G. Pardatscher, "Self-assembled active plasmonic waveguide with a peptide-based thermomechanical switch," ACS Nano **10**(12), 11377–11384 (2016).
35. F. N. Gür, C. P. T. McPolin, and S. Raza, "DNA-assembled plasmonic waveguides for nanoscale light propagation to a fluorescent nanodiamond," Nano Lett. **18**(11), 7323–7329 (2018).
36. A. T. M. Yesilyurt and J.-S. Huang, "Emission manipulation by DNA origami-assisted plasmonic nanoantennas," Adv. Opt. Mater. **9**(21), 2100848 (2021).
37. A. Kuzyk, R. Schreiber, and Z. Fan, "DNA-based self-assembly of chiral plasmonic nanostructures with tailored optical response," Nature **483**(7389), 311–314 (2012).
38. X. Shen, C. Song, and J. Wang, "Rolling up gold nanoparticle-dressed DNA origami into three-dimensional plasmonic chiral nanostructures," J. Am. Chem. Soc. **134**(1), 146–149 (2012).
39. A. Kuzyk, R. Schreiber, and H. Zhang, "Reconfigurable 3D plasmonic metamolecules," Nat. Mater. **13**(9), 862–866 (2014).
40. X. Shen, A. Asenjo-Garcia, and Q. Liu, "Three-dimensional plasmonic chiral tetramers assembled by DNA origami," Nano Lett. **13**(5), 2128–2133 (2013).
41. E. Winfree, F. Liu, L. A. Wenzler, *et al.*, "Design and self-assembly of two-dimensional DNA crystals," Nature **394**(6693), 539–544 (1998).
42. W. Liu, H. Zhong, R. Wang, *et al.*, "Crystalline two-dimensional DNA-origami arrays," Angew Chem. Int. Ed. **50**(1), 264–267 (2011).

Optics EXPRESS

43. A. Rajendran, M. Endo, and Y. Katsuda, "Programmed two-dimensional self-assembly of multiple DNA origami jigsaw pieces," ACS Nano **5**(1), 665–671 (2011).
44. Y. Suzuki, M. Endo, and H. Sugiyama, "Lipid-bilayer-assisted two-dimensional self-assembly of DNA origami nanostructures," Nat. Commun. **6**(1), 8052 (2015).
45. M. Endo, "Surface assembly of DNA origami on a lipid bilayer observed using high-speed atomic force microscopy," Molecules **27**(13), 4224 (2022).
46. A. Aghebat Rafat, T. Pirzer, and M. B. Scheible, "Surface-assisted large-scale ordering of DNA origami tiles," Angew Chem. Int. Ed. **53**(29), 7665–7668 (2014).
47. S. Woo and P. W. K. Rothemund, "Self-assembly of two-dimensional DNA origami lattices using cation-controlled surface diffusion," Nat. Commun. **5**(1), 4889 (2014).
48. C. Kielar, S. Ramakrishnan, and S. Fricke, "Dynamics of DNA origami lattice formation at solid–liquid interfaces," ACS Appl. Mater. Interfaces **10**(51), 44844–44853 (2018).
49. A. Xu, J. N. Harb, and M. A. Kostiainen, "DNA origami: The bridge from bottom to top," MRS Bull. **42**(12), 943–950 (2017).
50. P. Wang, S. Gaitanaros, and S. Lee, "Programming self-assembly of DNA origami honeycomb two-dimensional lattices and plasmonic metamaterials," J. Am. Chem. Soc. **138**(24), 7733–7740 (2016).
51. Y. Tian, T. Wang, and W. Liu, "Prescribed nanoparticle cluster architectures and low-dimensional arrays built using octahedral DNA origami frames," Nat. Nanotechnol. **10**(7), 637–644 (2015).
52. I. V. Martynenko, E. Erber, V. Ruider, *et al.*, "Site-directed placement of three-dimensional DNA origami," Nat. Nanotechnol. **18**, 1456–1462 (2023).
53. R. J. Kershner, L. D. Bozano, and C. M. Micheel, "Placement and orientation of individual DNA shapes on lithographically patterned surfaces," Nat. Nanotechnol. **4**(9), 557–561 (2009).
54. P. C. Waterman, "Symmetry, unitarity, and geometry in electromagnetic scattering," Phys. Rev. D **3**(4), 825–839 (1971).
55. R. N. S. Suryadharma and C. Rockstuhl, "Predicting observable quantities of self-assembled metamaterials from the T-matrix of its constituting meta-atom," Materials **11**(2), 213 (2018).
56. M. Schäferling, *Chiral Nanophotonics* (Springer International Publishing, 2017).
57. M. Hentschel, M. Schäferling, and X. Duan, "Chiral plasmonics," Sci. Adv. **3**(5), e1602735 (2017).
58. I. Fernandez-Corbaton, M. Fruhnert, and C. Rockstuhl, "Objects of maximum electromagnetic chirality," Phys. Rev. X **6**(3), 031013 (2016).
59. E. Prodan, C. Radloff, N. J. Halas, *et al.*, "A hybridization model for the plasmon response of complex nanostructures," Science **302**(5644), 419–422 (2003).
60. C. M. Domínguez, M. García-Chamé, and U. Müller, "Linker engineering of ligand-decorated DNA origami nanostructures affects biological activity," Small **18**(35), 2202704 (2022).
61. L. Schneider, K. S. Rabe, C. M. Domínguez, *et al.*, "Hapten-decorated DNA nanostructures decipher the antigen-mediated spatial organization of antibodies involved in mast cell activation," ACS Nano **17**(7), 6719–6730 (2023).
62. A. B. Khanikaev, N. Arju, and Z. Fan, "Experimental demonstration of the microscopic origin of circular dichroism in two-dimensional metamaterials," Nat. Commun. **7**(1), 12045 (2016).
63. X. Yin, M. Schäferling, B. Metzger, *et al.*, "Interpreting chiral nanophotonic spectra: The plasmonic Born–Kuhn model," Nano Lett. **13**(12), 6238–6243 (2013).
64. M. Esposito, V. Tasco, and M. Cuscunà, "Nanoscale 3D chiral plasmonic helices with circular dichroism at visible frequencies," ACS Photonics **2**(1), 105–114 (2015).
65. M. V. Gorkunov, A. A. Ezhov, and V. V. Artemov, "Extreme optical activity and circular dichroism of chiral metal hole arrays," Appl. Phys. Lett. **104**(22), 1 (2014).
66. R. Ogier, Y. Fang, and M. Svedendahl, "Macroscopic layers of chiral plasmonic nanoparticle oligomers from colloidal lithography," ACS Photonics **1**(10), 1074–1081 (2014).
67. P. Zhan, P. K. Dutta, and P. Wang, "Reconfigurable three-dimensional gold nanorod plasmonic nanostructures organized on DNA origami tripod," ACS Nano **11**(2), 1172–1179 (2017).
68. S. Pal, Z. Deng, and H. Wang, "DNA directed self-assembly of anisotropic plasmonic nanostructures," J. Am. Chem. Soc. **133**(44), 17606–17609 (2011).
69. W. Liu, L. Li, and S. Yang, "Self-assembly of heterogeneously shaped nanoparticles into plasmonic metamolecules on DNA origami," Chemistry A European J. **23**(57), 14177–14181 (2017).